

Article

A Global Assessment of Long-Term Greening and Browning Trends in Pasture Lands Using the GIMMS LAI3g Dataset

Benjamin I Cook ^{1,2,*} and Stephanie Pau ³

¹ NASA Goddard Institute for Space Studies, 2880 Broadway, New York, NY 10025, USA

² Lamont-Doherty Earth Observatory, 61 Route 9W, Palisades, NY 10964, USA

³ Department of Geography, Florida State University, 113 Collegiate Loop, Tallahassee, FL 32306, USA; E-Mail: spau@fsu.edu

* Author to whom correspondence should be addressed; E-Mail: benjamin.i.cook@nasa.gov; Tel.: +1-212-678-5669; Fax: +1-212-678-5552.

Received: 25 March 2013; in revised form: 2 May 2013 / Accepted: 7 May 2013 /

Published: 17 May 2013

Abstract: Pasture ecosystems may be particularly vulnerable to land degradation due to the high risk of human disturbance (e.g., overgrazing, burning, etc.), especially when compared with natural ecosystems (non-pasture, non-cultivated) where direct human impacts are minimal. Using maximum annual leaf area index (LAI_{max}) as a proxy for standing biomass and peak annual aboveground productivity, we analyze greening and browning trends in pasture areas from 1982–2008. Inter-annual variability in pasture productivity is strongly controlled by precipitation (positive correlation) and, to a lesser extent, temperature (negative correlation). Linear temporal trends are significant in 23% of pasture cells, with the vast majority of these areas showing positive LAI_{max} trends. Spatially extensive productivity declines are only found in a few regions, most notably central Asia, southwest North America, and southeast Australia. Statistically removing the influence of precipitation reduces LAI_{max} trends by only 13%, suggesting that precipitation trends are only a minor contributor to long-term greening and browning of pasture lands. No significant global relationship was found between LAI_{max} and pasture intensity, although the magnitude of trends did vary between cells classified as natural *versus* pasture. In the tropics and Southern Hemisphere, the median rate of greening in pasture cells is significantly higher than for cells dominated by natural vegetation. In the Northern Hemisphere extra-tropics, conversely, greening of natural areas is 2–4 times the magnitude of greening in pasture areas. This analysis presents one of the first global assessments of greening and browning trends in global pasture lands, including a comparison with vegetation trends in regions dominated by

natural ecosystems. Our results suggest that degradation of pasture lands is not a globally widespread phenomenon and, consistent with much of the terrestrial biosphere, there have been widespread increases in pasture productivity over the last 30 years.

Keywords: pasture; vegetation productivity; land degradation

1. Introduction

Pasture, defined as land cover used to support domesticated grazing livestock, represents the most widespread anthropogenic land use today [1]. Pastures cover approximately 25% of all global land areas [1,2], two and one half times the area cultivated for crops [3]. Over the last 300 years, the area of pasture coverage has expanded by an order of magnitude, from 324 million ha in 1700 C.E. to 3,429 million ha by 2000 C.E. [1,2], and pastures now provide 38% of the global net primary productivity appropriated for meat consumption and production [4]. Given their importance for both subsistence and commercial agriculture, it is critical to understand the extent to which pastures are experiencing long-term increasing (greening) or decreasing (browning) productivity trends and whether these changes can be attributed to climatic, anthropogenic, or other factors.

Global assessments using remotely sensed vegetation datasets have documented widespread greening and increased vegetation growth and productivity for many regions and ecosystems (e.g., [5–8]), including some pasture areas [9,10]. Of particular concern, however, is land degradation, generally defined as a sustained or persistent loss of ecological or biological productivity and ecosystem services due to disturbances arising from climate variations or human activities [11–13]. Characteristics of degraded ecosystems include reduced vegetation cover and productivity [12] and increased erosion [14], factors that can act to sustain or even amplify the initial degradation through a variety of processes (e.g., [12,15–19]). Pasture systems may be especially susceptible to land degradation due to the high risk of over-grazing [20,21] and extreme climate variations such as droughts [22,23]. Degraded pasture lands have been documented locally in many regions, including Africa [20], Asia [24], North America [25], and South America [26].

Since pastures are modified by human activities and are thus potentially under increased levels of stress due to disturbance and mismanagement, we might expect that pasture areas will be more susceptible to land degradation than natural (non-pasture, non-cultivated) ecosystems. To date, however, few studies have attempted a unified, global assessment of long-term greening and browning trends in pasture lands, including how productivity trends in pasture areas compare with natural ecosystems. Here we use a new, continuous (1981–2011) record of leaf area index (LAI), derived from satellite observations of the Normalized Difference Vegetation Index (NDVI), to investigate productivity trends in global pasture lands. We expand on previous work by analyzing pastures at the global scale using this new dataset, using multiple metrics for assessment of trend robustness, and quantifying climate contributions to trends over time. Specifically, we focus our analyses around the following research questions: (1) How strong, widespread, and significant are greening and browning trends in global

pasture lands? (2) What is the contribution of changes in climate (precipitation and temperature) to these trends? (3) How do trends in pasture areas compare with regions dominated by natural vegetation?

2. Methods and Material

2.1. Remote Sensing Data (*LAI3g*)

As a proxy for vegetation and ecosystem productivity, we use a new LAI dataset based on the third generation Global Inventory Modeling and Mapping Studies NDVI product (GIMMS NDVI3g) [27–29]. The GIMMS NDVI3g dataset is derived from the Advanced Very High Resolution Radiometer and is available at 8 km horizontal resolution every 10–15 days from 1981. GIMMS processing includes corrections for sensor calibration, volcanic aerosols, and other sensor degradation and contamination issues. It is the only continuous and up-to-date global NDVI dataset that is continually assessed and validated [30]. Globally, trends in the GIMMS NDVI3g compare favorably with trends derived from Landsat [31] and MODIS NDVI [32]. GIMMS is generally considered the best dataset to use for the analysis of long-term trends [30,31]. The GIMMS NDVI product has been used previously to diagnose and detect land degradation and greening trends (e.g., [11,30,33,34]).

LAI is defined as the green leaf area on the ground, expressed in units of m^2 leaf area per m^2 of ground. The derived LAI product [35] is generated based on a neural network algorithm that uses the GIMMS NDVI3g and an improved version of Collection 5 Terra MODIS LAI, the MODIS BNU product (Beijing Normal University version) [36]. This new LAI product (LAI3g) compares favorably with both ground based measurements of LAI and independent satellite estimates from the SPOT VEGETATION sensor [35,37], and also shows expected responses to temperature and precipitation variability [35]. For this study, we analyze the LAI3g dataset rather than the original NDVI3g data. LAI represents a variable that can be readily interpreted within an ecological context, while NDVI itself is a ratio of spectral reflectances that is a proxy for vegetation activity. As noted above, this LAI product has been verified using independent ground and satellite based LAI data. Our decision to analyze LAI instead of NDVI is also supported by precedent in the literature, including studies analyzing satellite vegetation trends using variables derived from NDVI, instead of NDVI directly (e.g., [38–40]).

We use maximum annual values of LAI (LAI_{max}) as a proxy for standing biomass and peak annual aboveground productivity. Maximum annual NDVI/LAI has been used previously to investigate long-term greening and browning trends (e.g., [24,41,42]). Alternative approaches have used NDVI/LAI integrated annually or over the growing season (e.g., [11]). Objectively defining the growing season using remotely sensed vegetation products can be difficult, however, especially in areas where the timing and length of the growing season varies significantly from year to year [41]. Additionally, neither proxy considers belowground carbon allocation, *i.e.*, root/shoot ratio [43].

Given that maximum and integrated values of NDVI/LAI are often strongly and positively correlated (e.g., [41]), we believe LAI_{max} provides the most straightforward proxy indicator of aboveground biomass and productivity that is appropriate for our analyses. For the Northern Hemisphere, we calculate LAI_{max} based on the year from January to December; for the Southern Hemisphere, we use July to June.

We calculate LAImax at each 8 km resolution grid cell, and then spatially average all LAImax cells to create a new dataset at 0.5° spatial resolution, the same resolution as our climate and land cover datasets.

2.2. Land Cover Data

Three estimates of the modern and historical distribution of human land use and land cover (including pastures) are available in the literature [44]: (1) Houghton (2008) (HH, [45]); (2) HYDE 3.1 (HYDE, [46]); and (3) an updated version of Ramankutty and Foley (1999) (RF, [47]). Land cover datasets are from Meiyappan and Jain (2012) [44], and were obtained from [48]. For pasture land, substantial differences can be seen in the distribution and intensity of this land use type across the three datasets (Figure 1). The HH estimate represents the major outlier, showing significantly lower pasture areas than both HYDE and RF. The HH calculation assumes that, outside of Latin America, all pastures are derived from grasslands and forests are never converted to pastures, leading to a severe underestimation of pasture land extent. Globally, pasture estimates from HYDE and RF are similar, although significant differences are still apparent for many regions, including Africa, Australia, the Middle East, and Asia (Figure 2). Differences between HYDE and RF are primarily due to the underlying data used in the land cover reconstruction. RF uses a census report with significantly lower pasture areas than the FAO estimate [49] used in HYDE, leading to much more widespread and intensive pasture distributions in HYDE relative to RF. Since HYDE represents the most recent and up-to-date estimate of modern and historical pasture areas, we use this dataset to discriminate between pasture and non-pasture regions in our analysis. Specifically, we distinguish between cells that are natural (<10% pasture), low intensity pasture ($\geq 10\% - < 50\%$ pasture), and high intensity pasture ($\geq 50\%$ pasture).

Figure 1. Modern day distributions of pasture areas (units of percent cover) from three different land cover datasets: (a) HH [45]; (b) HYDE [46]; and (c) RF (updated from [47]). Shown are the distributions from the most recent year available in each dataset, as indicated in the title of each panel.

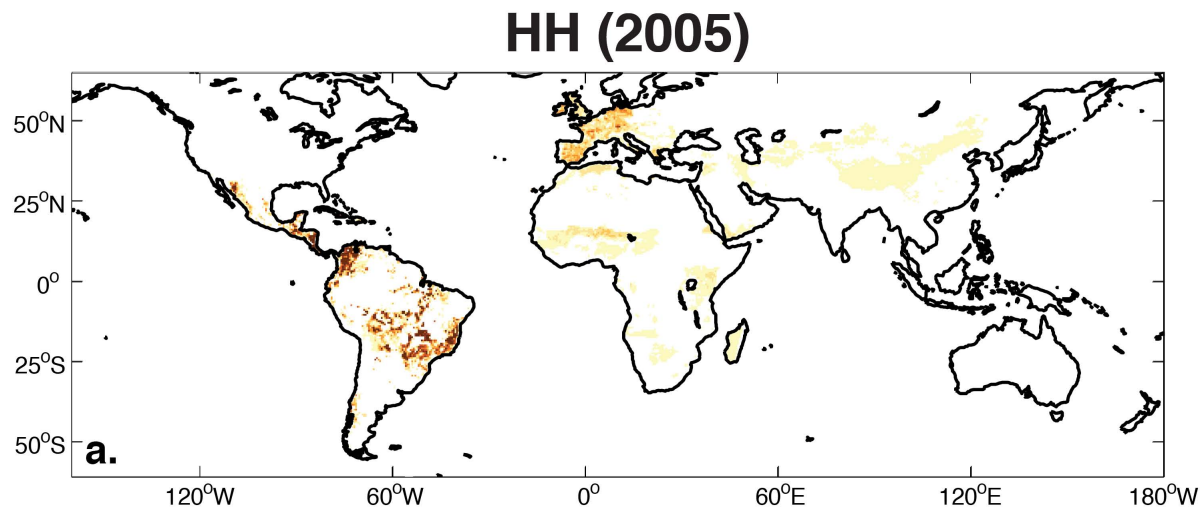


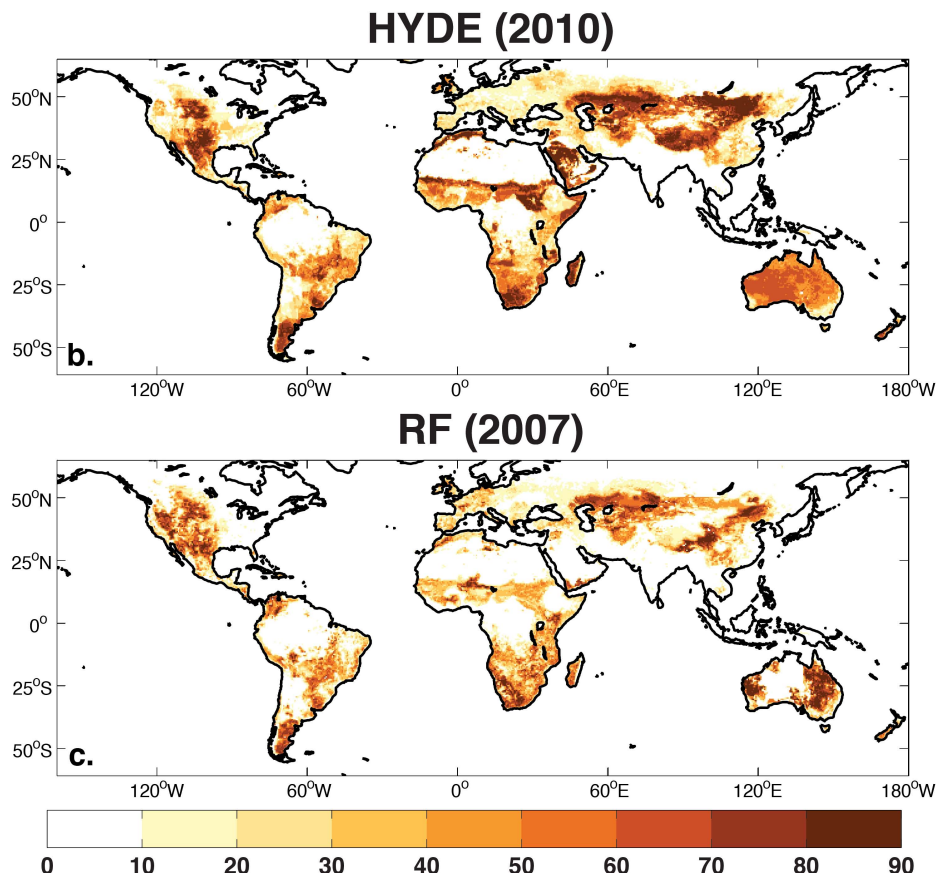
Figure 1. Cont.

Figure 2. Difference in pasture area (percent of cell) between the HYDE and RF datasets for the latest year available from both datasets (2007). Areas in orange to red are regions where HYDE has greater pasture area than RF; purple areas are where pasture area in RF exceeds that of HYDE. Overall, HYDE indicates more widespread pasture areas than RF, especially in Asia, Africa, the Middle East, and central Australia. RF pasture area is larger in more localized areas, including western North America, Europe, and far eastern and western Australia.

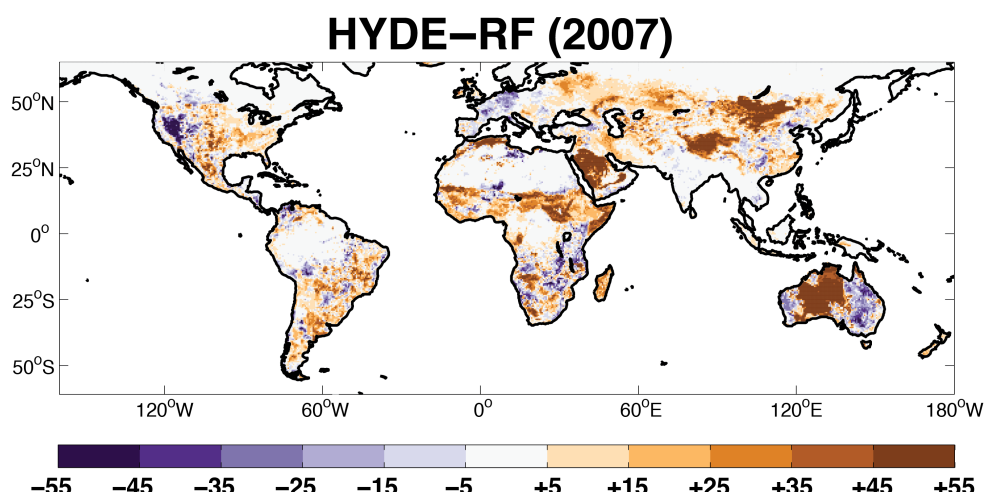
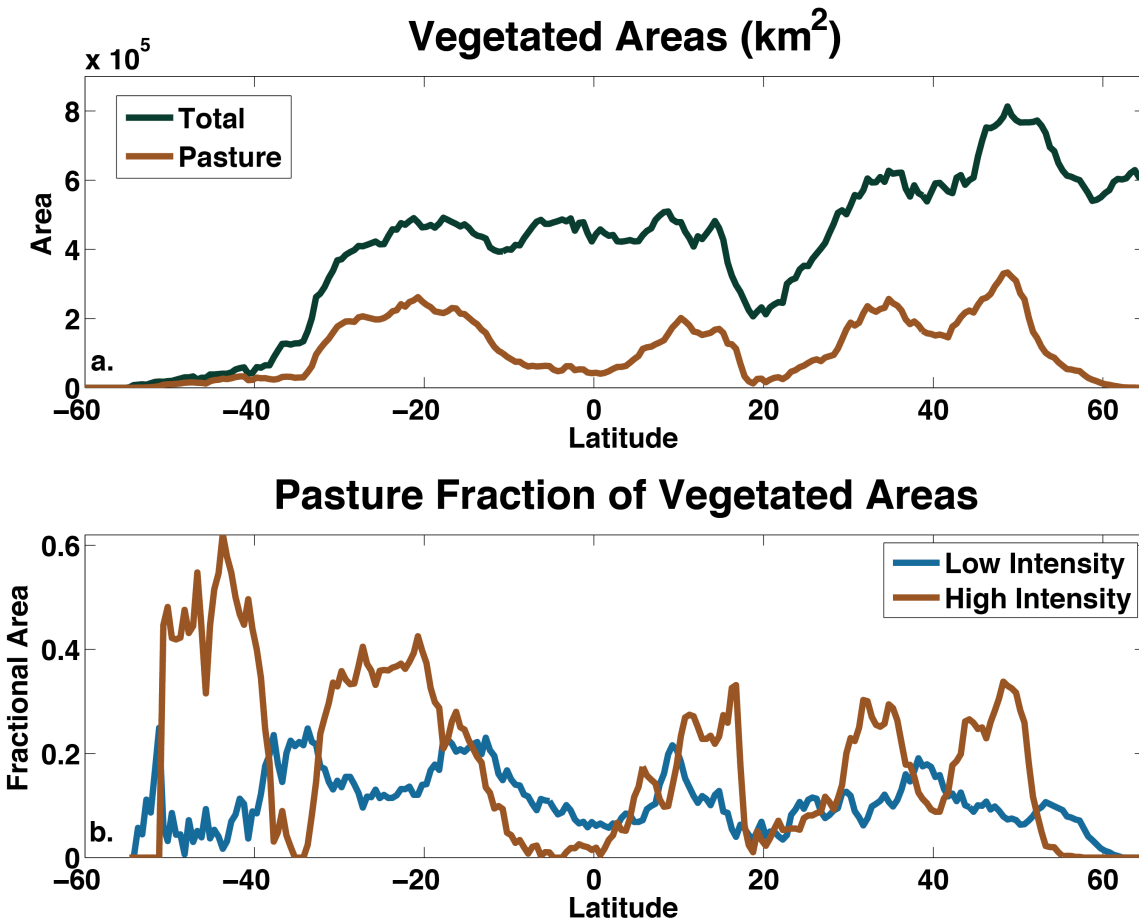


Figure 3. Latitudinal distribution of pasture areas from the HYDE3.1 dataset: (a) total vegetated and pasture areas (km^2) and (b) fraction of vegetated areas covered by low intensity ($\geq 10\%$ to $\leq 50\%$ percent cover) and high intensity pasture ($> 50\%$ percent cover).



Globally, the most extensive pasture regions are concentrated in the subtropics of both hemispheres and the mid-latitudes of the Northern Hemisphere (Figure 3(a)). Local minima occur in the tropics, where the landscape is dominated by tropical forests, and around 20°N, corresponding to the latitudinal band containing the Sahara desert and much of monsoon Asia, where the landscape is dominated by cultivated agriculture. Pastures represent the dominant fraction of total vegetated areas in much of the Southern Hemisphere extra-tropics (Figure 3(b)), as well as significant fractions of the total vegetation in the Northern Hemisphere tropics (0°N–20°N) and mid-latitudes.

2.3. Climate Data

For climate data, we use an updated version of the monthly climate grids (version 3.1) available from the Climate Research Unit (CRU) at the University of East Anglia [50]. These data, representing monthly precipitation and temperature, are available for 1901–2009, and cover all global land areas (excluding Antarctica) at 0.5° horizontal resolution. Gridded values are based upon a statistical interpolation from individual weather stations. For comparisons with LAI_{max}, we convert the monthly data to annual means (for temperature) and annual sums (for precipitation), using seasonal intervals consistent

with the calculation of LAImax (January–December for the Northern Hemisphere; July–June for the Southern Hemisphere).

2.4. Analysis

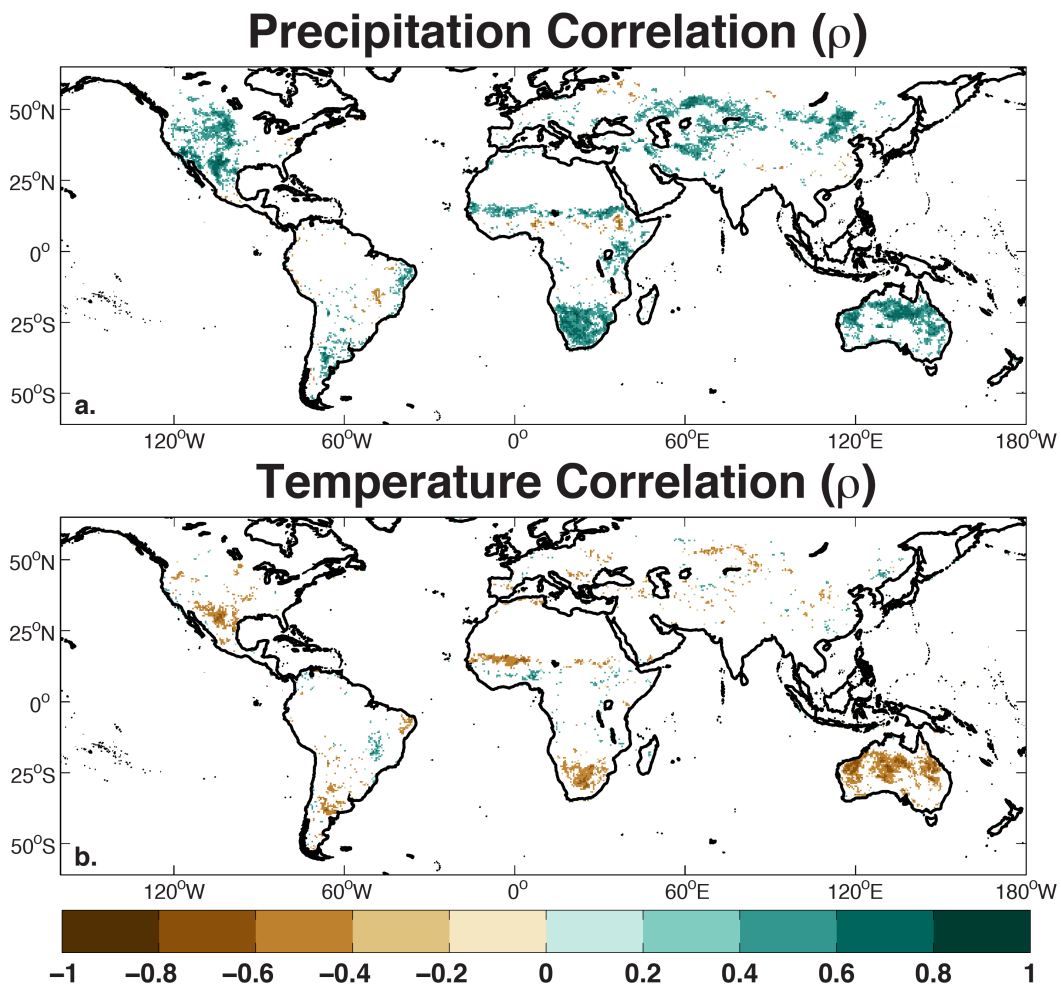
Spatially, we restrict our analysis to all latitudinal bands between 60°S and 60°N, within which nearly all of the pasture areas are contained. Temporally, we restrict our analyses to the common time periods available from all datasets (1982–2008) and use land cover from the HYDE dataset for 2008. To quantify climate controls on pasture productivity, we calculate Spearman’s rank correlation coefficient (ρ) between the linearly detrended climate variables (annual temperature and precipitation) and LAImax. Spearman’s ρ is defined as the Pearson correlation coefficient (r) of two ranked variables, is bounded between -1 and $+1$ (same interpretation as Pearson’s r), and is less sensitive than Pearson’s r to outliers. To investigate temporal trends in LAImax, we calculate linear trends (1982–2008) using three methods: a best fit ordinary least squares linear regression, Spearman’s ρ , and Kendall’s τ . Kendall’s τ is a non-parametric test (as is Spearman’s ρ) for rank correlation between two variables, calculated as the difference between the number of concordant and discordant pairs in the ranked bivariate data (*i.e.*, LAImax *versus* time), divided by the total number of possible pair combinations of the ranked data. As with the Pearson’s and Spearman correlation coefficients, Kendall’s τ is bounded between -1 and $+1$. A value of $+1$ indicates perfect agreement (*i.e.*, correlation) among the two rankings; a value of -1 indicates perfect disagreement (*i.e.*, anti-correlation). We consider temporal trends in LAImax to be robust if trend estimates from all three tests pass a significance threshold of $p \leq 0.05$. To minimize the influence of cultivated crop areas, we ignore any cells containing greater than 30% crop area, using crop fractions from the HYDE dataset. To compare trends spatially, we additionally stratify the data based on latitudinal bands: the Southern Hemisphere extra-tropics (60°S–20°S), the tropics (20°S–20°N), and the Northern Hemisphere extra-tropics (20°N–60°N).

3. Results

3.1. Correlation with Climate

Precipitation is the dominant climate control on inter-annual variability of LAImax in pasture cells, showing widespread and significant positive correlations, especially in semi-arid regions (Figure 4(a)). Significant correlations with temperature are less extensive and mostly negative (Figure 4(b)). Regions exhibiting negative temperature correlations generally overlap with areas of significant positive precipitation correlation, suggesting that warmer temperatures may cause increased moisture stress. Additionally, the regions correlated with temperature are generally not core tropical regions where plants are more likely near their temperature optimum, *i.e.*, areas where we might expect a negative relationship with temperature because of increases in respiration or photorespiration [51]. Inter-annual variability in pasture LAImax therefore appears to be limited primarily by moisture, rather than by temperature.

Figure 4. Correlation (Spearman's ρ) between LAImax of pasture cells and (a) annual total precipitation and (b) annual mean temperature for 1982–2008. Insignificant correlations ($p > 0.05$) have been masked out. Correlations are based on linearly detrended time series of LAImax, temperature, and precipitation.

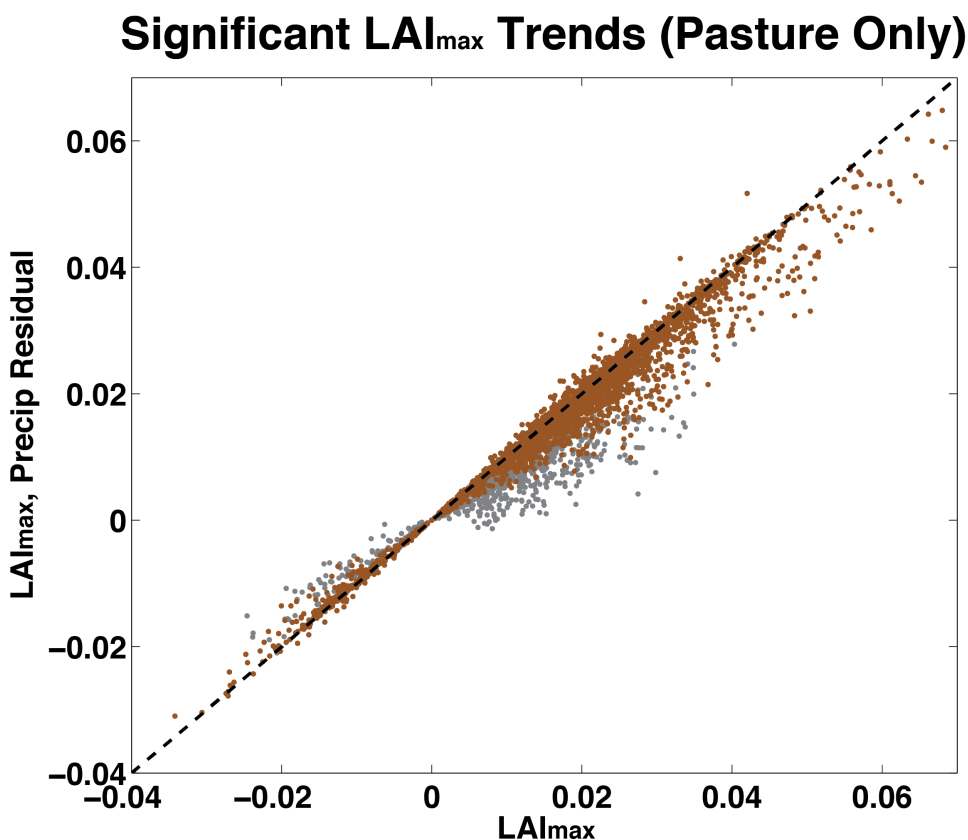


3.2. Global Trends

Globally, 23.4% of cells with $\geq 10\%$ pasture cover have significant temporal trends for 1982–2008, based on our three trend test significance criteria. Similar results are found if we calculate trends on the residuals after the influence of annual precipitation on LAImax has been removed using a simple linear regression (21.7% of pasture cells). Removing the influence of temperature has little effect, consistent with the generally weaker and less widespread temperature correlations (not shown). The absolute magnitude of the trends (both negative and positive) is reduced when the precipitation signal is statistically removed (Figure 5), implying some contributing effect of precipitation toward long-term greening and browning in pastures. Averaged across cells, however, the trend is only slightly diminished: +0.0162 and +0.0155 m^2/m^2 per year before and after removal of the precipitation signal, respectively. For cells with significant LAImax trends, the precipitation detrending decreases the magnitude of the LAImax trends by an average of 12.9%. Given the similarity in magnitude and direction of the LAImax trends with and without removal of the precipitation signal, this suggests that recent precipitation trends

are only a minor contributor to productivity trends in pasture areas over the last 30 years. Comparisons between LAImax trends and fractional pasture coverage show no significant global relationship between the magnitude of the LAImax trends and time averaged (1982–2008) pasture intensity. We also found no relationship between LAImax trends and temporal changes in pasture cover intensity over this interval.

Figure 5. Comparisons of significant LAImax trends calculated for pasture cells (*i.e.*, cells with $\geq 10\%$ pasture cover) for trends calculated before (x-axis) and after (y-axis) detrending the influence of annual precipitation. The 1:1 line is black and dashed, representing identical trends between the two methods. Cells for which trends became insignificant after precipitation detrending are in grey.



Pasture and natural vegetation regions show a mixture of browning and greening trends (Figure 6, no significance masking). For natural vegetation (Figure 6(a)), the most cohesive regions of greening are found in tropical regions of South America and Africa, while the high northern latitudes show a mix of greening and browning trends. For pasture areas (Figure 6(b)), general trends are towards increasing LAImax, with localized areas of browning in southeast Australia, Mongolia and central China, western North America, east Africa, southern Africa, and southern South America. However, much of the browning in both the natural and pasture vegetation cells disappears when we apply our three significance test filtering (Figure 7), and greening dominates the significant trends in both natural vegetation and pasture systems. Strongest trends towards greening in pasture areas are found in West Africa and South America, while productivity declines are most apparent in Australia, western North America, and central China and Mongolia.

Figure 6. Percent change in LAI_{max} (1982–2008) for all (a) natural (<10% pasture cover) and (b) pasture ($\geq 10\%$ pasture cover) vegetated cells, with no significance masking. Cells with $\geq 30\%$ cultivated crop fractions have been masked out.

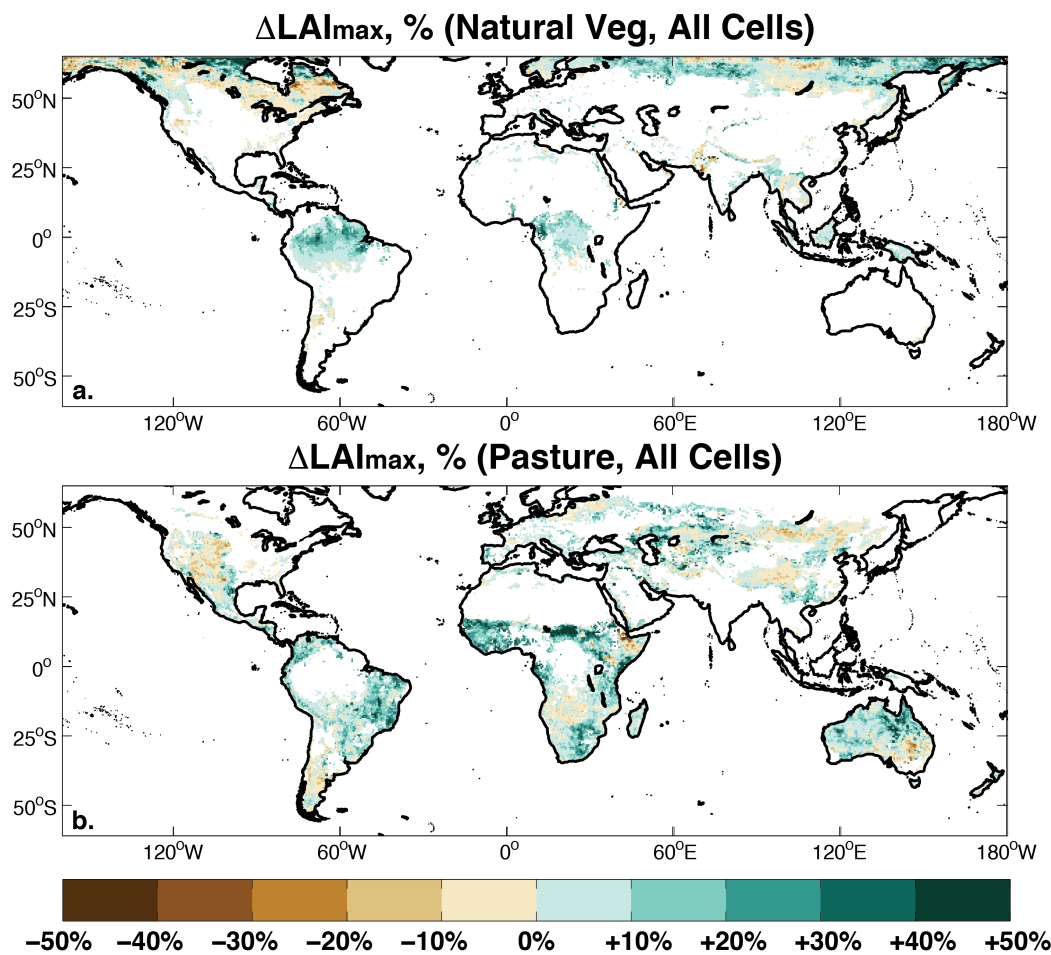


Figure 7. Percent change in LAI_{max} (1982–2008) for all (a) natural (<10% pasture cover) and (b) pasture ($\geq 10\%$ pasture cover) vegetated cells, with insignificant regions masked based on the three trend test criteria. Cells with $\geq 30\%$ cultivated crop fractions have been masked out.

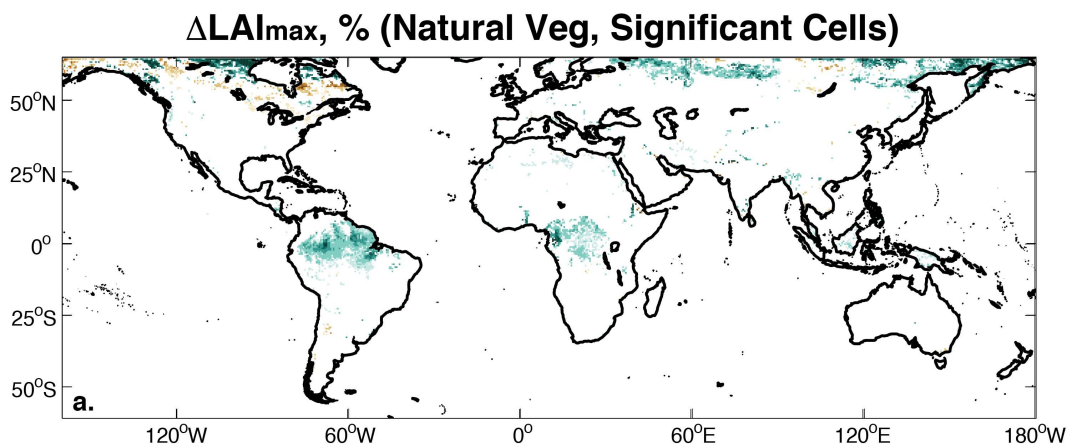
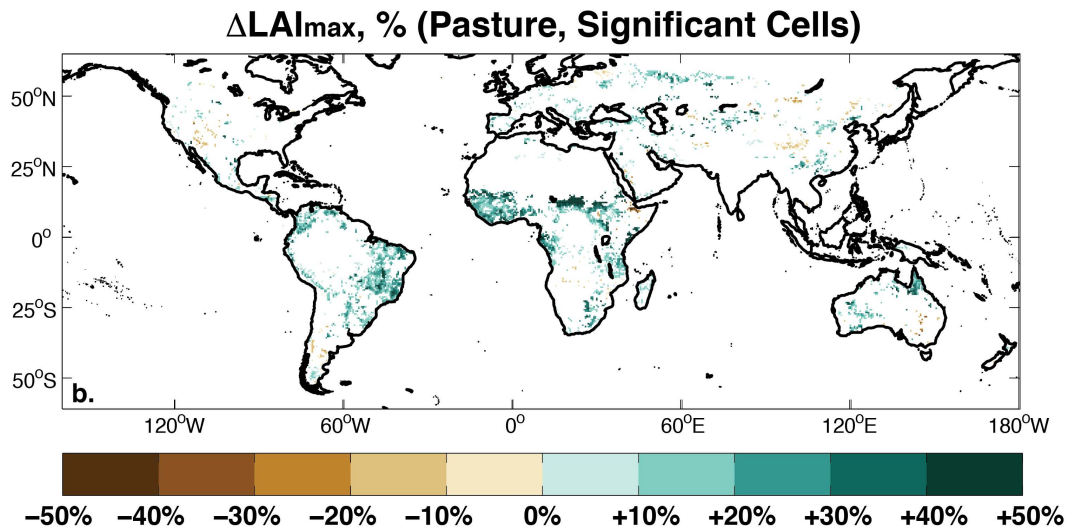


Figure 7. Cont.

3.3. Spatial Variability

Changes in LAI_{max} vary across latitudinal bands and between natural vegetation, low-intensity pasture, and high-intensity pasture areas. This can be seen in the cumulative distribution functions (CDFs) for each latitudinal band and vegetation classification (in Figure 8). Consistent with the global analysis, greening trends dominate among all three vegetation types and across all three latitudinal bands. In the Southern Hemisphere extra-tropics (60°S – 20°S), greening trends are higher in pasture cells *versus* regions with natural vegetation. This may reflect a sample bias, since natural vegetation makes up a relatively small fraction of the vegetated areas in the Southern Hemisphere extra-tropics (Figure 3(b)). The same general pattern holds for the tropics (20°S – 20°N), where pasture cells are greening much more than natural vegetated areas. A look at the cdfs (Figure 8(c,d)) suggests that differences in the tropics are driven primarily by differences among the most rapidly greening cells. The situation reverses in the Northern Hemisphere extra-tropics (20°N – 60°N), where cells with natural vegetation are increasing their greenness at a much higher rate than pastures. Except for the tropics, differences in the CDFs are generally reflected in the median trends for each vegetation type (Figure 9). Greatest differences across vegetation types are seen in the Northern Hemisphere extra-tropics, where cells with natural vegetation and significant trends are greening at 2–4 times the rate of pasture cells.

These differences can be confirmed quantitatively by comparing the trend distributions using a two sample Kolmogorov–Smirnov (KS) test (a non-parametric goodness of fit test applied to the cdfs) and a two sample Wilcoxon rank-sum (WR) test for differences in the median. For the tropics and Southern Hemisphere extra-tropics, the KS and WR tests confirm that low and high intensity pasture areas are greening at a greater rate than natural vegetated areas ($p < 0.001$). For the Northern Hemisphere extra-tropics, the KS and WR tests indicate that natural vegetated areas are greening at a higher rate than low or high intensity pasture areas ($p < 0.001$). These results and their significance levels are similar whether these tests are applied to the cdfs with or without the three trend test significance masking.

Figure 8. Cumulative distribution functions (CDFs) for percent changes in LAImax (1982–2008), stratified by latitudinal band and vegetation cover (natural, low-intensity pasture, and high-intensity pasture): the Southern Hemisphere extra-tropics (60°S – 20°S ; (a,b)); the tropics (20°S – 20°N ; (c,d)); and the Northern Hemisphere extra-tropics (20°N – 60°N ; (e,f)). CDFs in the left column are for all cells of each land cover type; CDFs in the right column include only those cells that pass the three trend test criteria.

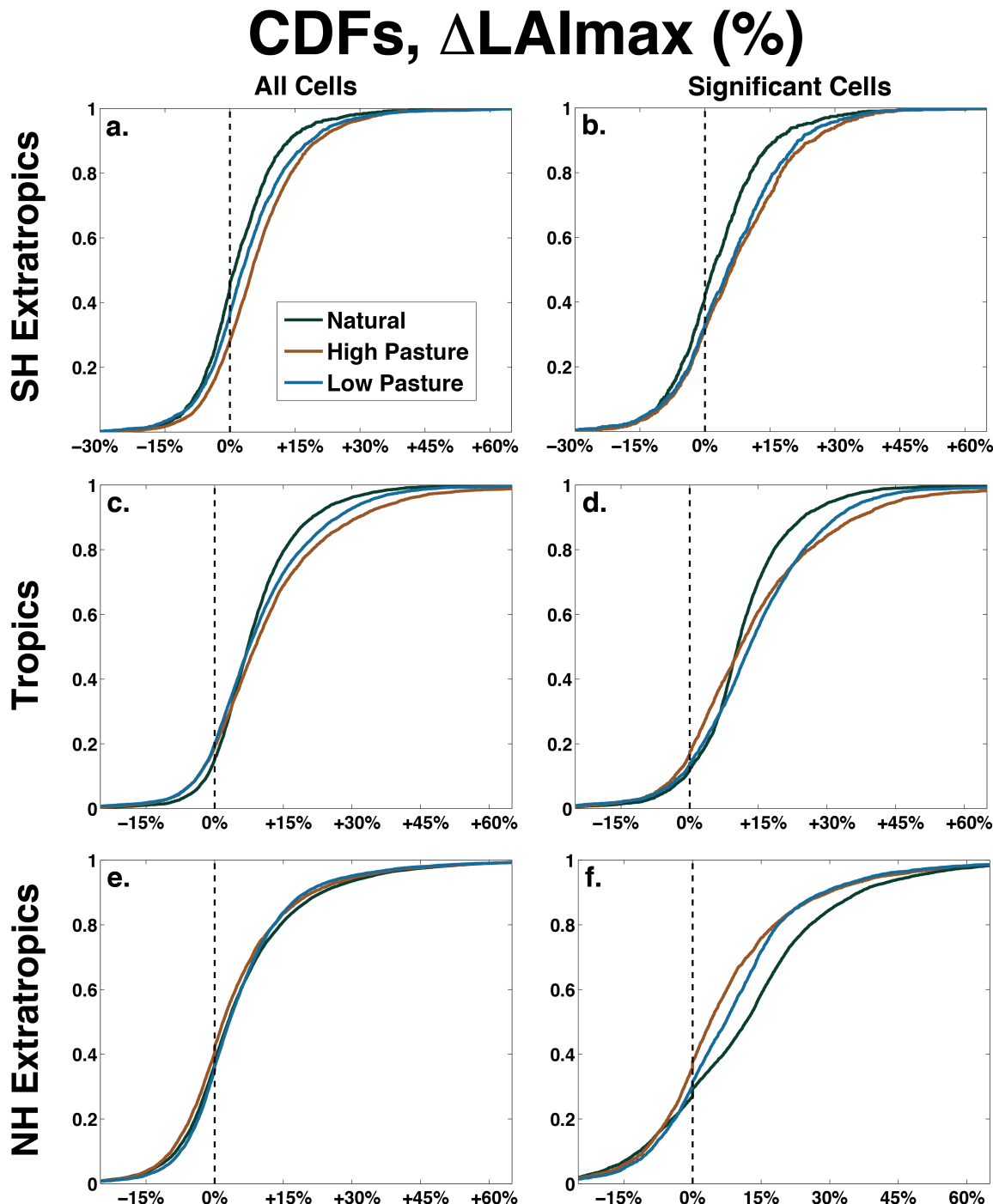
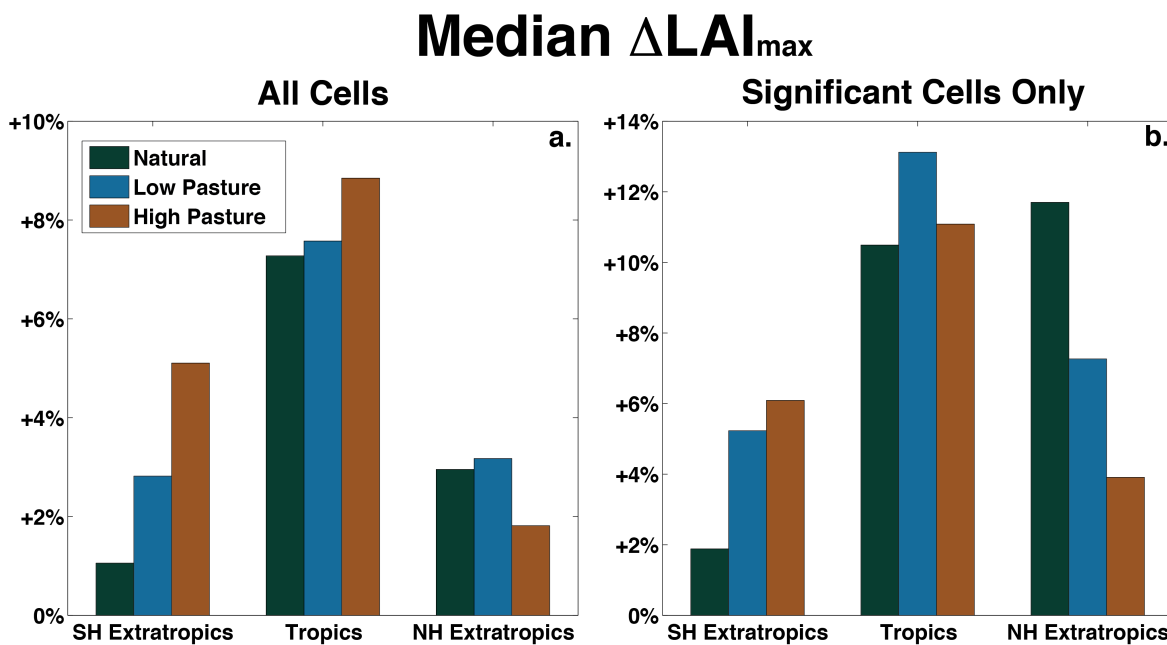


Figure 9. Median change in LAI_{max} for each latitudinal band, calculated across (a) all qualifying cells and (b) only those cells that pass the three trend test significance criteria.



4. Discussion

We focus on productivity trends in global pasture lands, the most widespread human land use type and one that may be especially prone to land degradation and desertification because of the potential for overexploitation [52,53]. We find that roughly one quarter of pasture cells in the GIMMS LAI3g dataset show significant greening or browning trends in 1982–2008, with the vast majority of significantly trending cells showing greening and increased productivity. The sign and magnitude of the productivity trends, whether greening or browning, are unrelated to the intensity of pasture or changes in pasture area within any given grid cell, and precipitation appears to be only a minor contributor to overall productivity trends. Notably, our results suggest that: (1) degradation of pastures is not a globally widespread phenomenon; (2) the occurrence and magnitude of degradation and declining productivity trends is not significantly higher in pasture regions compared with natural ecosystems; and (3) the long-term greening of pastures is similar to trends observed for natural vegetation, albeit with different spatial fingerprints in different regions.

Our results are broadly consistent with previous studies that have documented widespread greening and increased productivity in the biosphere over the last several decades (e.g., [6,7,35,54]). These increases have largely been attributed to increased temperatures and longer growing seasons, especially at high latitudes (e.g., [55,56]), and recovery from major disturbances, such as the Sahel drought of the 1970s [57,58]. At the local and regional scale, however, there is greater disagreement in the literature on the magnitude and direction of vegetation trends, especially regarding land degradation and productivity declines. In their global analysis of net primary productivity trends in 1982–2003, Bai *et al.* (2008) [11] found large, widespread declines in vegetation productivity in regions that would qualify as pastures in our analysis, including large areas in the Southern Hemisphere, Asia, and North America. While we

find some productivity declines in these same regions (Figure 6), our analyses indicate that the areas of significant decline are much more localized (Figure 7). Disagreement between our study and Bai *et al.*'s finding may be due to significant methodological differences between the two studies [59]. For example, Bai *et al.* did not filter out areas of cultivated agriculture, only analyzed trends up to 2003, and used January–December as their calendar year for the Southern Hemisphere.

For areas where we do find significant and relatively widespread browning and productivity declines (Asia, southwestern North America, southeast Australia), this degradation is largely corroborated by other studies. In Mongolia and Central Asia, increased population pressure and land exploitation have led to significant vegetation mortality and desertification in recent decades [24,60,61]. In southwestern North America, net primary productivity has been declining [62], possibly due to recent climatic changes. In southeastern Australia, the recent “Millennium Drought” [63] has driven significant vegetation productivity declines [64–66]. Other areas where we do not find significant and widespread degradation, but where degradation has been independently documented, include Africa [20] and South America [26,67].

Furthermore, it should be noted that many studies using either ground observations or higher resolution remote sensing data have locally documented significant pasture degradation for many regions, including areas where our analysis indicates greening or no change (e.g., [68,69]). This suggests that there may be some disconnection between low resolution global studies and higher resolution, more localized analyses for documenting land degradation. For example, Miehle *et al.* (2010) [20] found significant land degradation at a local, long-term field site; this degradation was not apparent from remote sensing observations of the area. Independently, Le *et al.* (2012) [70] found that, for a river basin in West Africa, CO₂-enhanced vegetation productivity trends actually masked the true scale of soil loss and degradation in the basin. This is consistent with other studies that suggest large scale or regional greening trends may act to mask local degradation [10]. Ultimately, a comprehensive accounting of global land degradation and productivity trends in pasture lands will require a coherent and unified assessment using both local and regional information on productivity and pasture intensity and management.

Several hypotheses may explain why pasture areas are greening on average, despite recent climatic shifts and increases in their exploitation intensity. Atmospheric carbon dioxide (CO₂) concentrations have increased significantly over the last 150 years, possibly driving a fertilization effect that has resulted in increases in productivity by either directly enhancing photosynthesis or indirectly increasing water use efficiency [71,72]. Indeed, several studies using remote sensing data have at least partially attributed greening trends in various regions to CO₂ fertilization [73,74]. However, the true magnitude of the CO₂ fertilization effect is highly uncertain, with large disagreement among experimental and modeling studies (e.g., [75–77]). Another possibility is shrub encroachment, a widespread phenomena in both temperature and moisture limited grasslands where native grasses are being progressively replaced by shrub vegetation (e.g., [78]). Shrub encroachment has been documented in many regions dominated by pasture ecosystems, including North America, Africa, Australia, and South America (see [79] for a review). Initial research indicated that shrub encroachment caused reduced productivity and an overall loss of ecosystem function [18,80]. More recent work, however, suggests that the functional consequences of shrub encroachment are more mixed [81], with several studies indicating shrub encroachment can lead to increases in productivity or even reverse land degradation processes [82–84],

especially in more mesic grasslands [85]. Finally, because successional dynamics often operate on time scales longer than the satellite record (*i.e.*, decades to centuries), greening trends from satellites may represent recovery from disturbance events. Examples of such disturbances include fire [86], drought [57,58], and insects [62], all of which may give the appearance of longer term greening trends if they occur near the beginning of the satellite record.

5. Conclusions

Using a new, satellite based dataset of leaf area index, we conducted one of the first global scale analyses of long-term productivity trends in pasture lands. We found significant trends in nearly one quarter of all pasture grid cells, with most significantly trending cells increasing their productivity in 1982–2008. Median increases across pasture grid cells were on the order of 5%–10%, and the most spatially extensive greening was found in South America, Africa, and localized areas of Asia and Australia. In the tropics and Southern Hemisphere, pasture areas greened faster than areas dominated by natural vegetation, while in the Northern Hemisphere areas of natural vegetation greened at a rate of 2–4 times that of pastures. Areas of significant browning were much more isolated, occurring predominately in China, Mongolia, and Australia, suggesting that land degradation and desertification of pasture lands is not a globally widespread phenomenon. Trends in precipitation and temperature explain only a minor fraction of overall pasture productivity trends, and pasture intensity was unrelated to productivity trends. While it is difficult in this analysis to ascribe any specific causes, the available literatures suggest that several non-climatic factors may explain some of the regional trends, including plant successional dynamics and CO₂ fertilization.

Our analysis provides a broad overview of trends and variability in pasture lands, the most widespread human land use type, at the global scale. Reconciling these results across multiple spatial and temporal scales (*e.g.*, [20,87]) and disentangling the relative importance of various drivers [20,58,88,89] remains a significant challenge. Improving our understanding of pasture productivity trends and their drivers will require the use of expanded data sets that can provide additional information and help explain the geographic patterns of greening. These data could include information on stocking rates, fallow periods, burn frequency, and other management protocols that would potentially affect productivity and vegetation cover in pasture ecosystems. These additional data, combined with a conceptual framework for bridging coarse global analyses with detailed localized studies, will be critical for providing additional insights on the productivity trends in global pasture lands.

Acknowledgements

The LAI3g data were graciously provided by Ranga Myneni and Zhaichun Zhu. Support for BI Cook came from NASA. The authors thank four anonymous reviewers whose comments greatly improved the quality of this manuscript. LDEO contribution #7691.

References

1. Pielke, R.A.; Pitman, A.; Niyogi, D.; Mahmood, R.; McAlpine, C.; Hossain, F.; Goldewijk, K.K.; Nair, U.; Betts, R.; Fall, S.; et al. Land use/land cover changes and climate: Modeling analysis and observational evidence. *Wiley Interdiscip. Rev. Clim. Chang.* **2011**, *2*, 828–850.
2. Turner, B.L.; Clark, W.C.; Kates, R.W.; Richards, J.F.; Mathews, J.T.; Meyer, W.B. *The Earth as Transformed by Human Action: Global and Regional Changes in the Biosphere over the Past 300 Years*; Cambridge University Press: Cambridge, UK, 1991.
3. Tubiello, F.N.; Soussana, J.F.; Howden, S.M. Crop and pasture response to climate change. *Proc. Natl. Acad. Sci.* **2007**, *104*, 19686–19690.
4. Imhoff, M.L.; Bounoua, L.; Ricketts, T.; Loucks, C.; Harriss, R.; Lawrence, W.T. Global patterns in human consumption of net primary production. *Nature* **2004**, *429*, 870–873.
5. Hüttich, C.; Herold, M.; Schmullius, C.; Egorov, V.; Bartalev, S.A. Indicators of Northern Eurasia’s land cover change trends from SPOT-VEGETATION time-series analysis 1998–2005. *Int. J. Remote Sens.* **2007**, *28*, 4199–4206.
6. Nemani, R.R.; Keeling, C.D.; Hashimoto, H.; Jolly, W.M.; Piper, S.C.; Tucker, C.J.; Myneni, R.B.; Running, S.W. Climate-driven increases in global terrestrial net primary production from 1982 to 1999. *Science* **2003**, *300*, 1560–1563.
7. Slayback, D.A.; Pinzon, J.E.; Los, S.O.; Tucker, C.J. Northern hemisphere photosynthetic trends 1982–99. *Glob. Chang. Biol.* **2003**, *9*, 1–15.
8. Xiao, J.; Moody, A. Geographical distribution of global greening trends and their climatic correlates: 1982–1998. *Int. J. Remote Sens.* **2005**, *26*, 2371–2390.
9. Fensholt, R.; Rasmussen, K. Analysis of trends in the Sahelian rain-use efficiency using GIMMS NDVI, RFE and GPCP rainfall data. *Remote Sens. Environ.* **2011**, *115*, 438–451.
10. Nutini, F.; Boschetti, M.; Brivio, P.A.; Bartholomé, E.; Hoscilo, A.; Stroppiana, D.; Bocchi, S. Analysis of vegetation pasture climate response on Sahel Region through 10 years of remotely sensed data. *Proc. SPIE* **2010**, *7824*, doi:10.1117/12.865205.
11. Bai, Z.G.; Dent, D.L.; Olsson, L.; Schaepman, M.E. Proxy global assessment of land degradation. *Soil Use Manag.* **2008**, *24*, 223–234.
12. D’Odorico, P.; Bhattachan, A.; Davis, K.F.; Ravi, S.; Runyan, C.W. Global desertification: Drivers and feedbacks. *Adv. Water Resour.* **2013**, *51*, 326–344.
13. Millennium Ecosystem Assessment (MEA). *Ecosystems and Human Well-Being*; World Resources Institute/Island Press: Washington, DC, USA, 2005.
14. Wolfe, S.A.; Nickling, W.G. The protective role of sparse vegetation in wind erosion. *Progr. Phys. Geogr.* **1993**, *17*, 50–68.
15. Charney, J.G. Dynamics of deserts and drought in the Sahel. *Quart. J. R. Meteorol. Soc.* **1975**, *101*, 193–202.
16. Charney, J.; Quirk, W.J.; Chow, S.H.; Kornfield, J. A comparative study of the effects of albedo change on drought in semi-arid regions. *J. Atmos. Sci.* **1977**, *34*, 1366–1385.
17. Cook, B.I.; Miller, R.L.; Seager, R. Amplification of the North American “Dust Bowl” drought through human-induced land degradation. *Proc. Natl. Acad. Sci. USA* **2009**, *106*, 4997–5001.

18. Schlesinger, W.H.; Reynolds, J.F.; Cunningham, G.L.; Huenneke, L.F.; Jarrell, W.M.; Virginia, R.A.; Whitford, W.G. Biological feedbacks in global desertification. *Science* **1990**, *247*, 1043–1048.
19. Yoshioka, M.; Mahowald, N.M.; Conley, A.J.; Collins, W.D.; Fillmore, D.W.; Zender, C.S.; Coleman, D.B. Impact of desert dust radiative forcing on sahel precipitation: Relative importance of dust compared with sea surface temperature variations, vegetation changes, and greenhouse gas warming. *J. Clim.* **2007**, *20*, 1445–1467.
20. Miehe, S.; Kluge, J.; Von Wehrden, H.; Retzer, V. Long-term degradation of Sahelian rangeland detected by 27 years of field study in Senegal. *J. Appl. Ecol.* **2010**, *47*, 692–700.
21. Ravi, S.; Breshears, D.D.; Huxman, T.E.; D’Odorico, P. Land degradation in drylands: Interactions among hydrologic-aeolian erosion and vegetation dynamics. *Geomorphology* **2010**, *116*, 236–245.
22. Nicholson, S.E.; Tucker, C.J.; Ba, M.B. Desertification, drought, and surface vegetation: An example from the West African sahel. *Bull. Am. Meteorol. Soc.* **1998**, *79*, 815–829.
23. Weaver, J. E.; Albertson, F. W. Effects on the great drought on the Prairies of Iowa, Nebraska, and Kansas. *Ecology* **1936**, *17*, 567–639.
24. Li, A.; Wu, J.; Huang, J. Distinguishing between human-induced and climate-driven vegetation changes: A critical application of RESTREND in inner Mongolia. *Landsc. Ecol.* **2012**, *27*, 969–982.
25. Worster, D. *Dust Bowl: The Southern High Plains in the 1930s*; Oxford University Press: Oxford, UK, 1979.
26. McConnell, J.; Aristarain, A.; Banta, J.; Edwards, P.; Simões, J. 20th-Century doubling in dust archived in an Antarctic Peninsula ice core parallels climate change and desertification in South America. *Proc. Natl. Acad. Sci. USA* **2007**, *104*, 5743–5748.
27. Pinzon, J.; Brown, M.; Tucker, C.J. EMD Correction Of Orbital Drift Artifacts in Satellite Data Stream. In *Hilbert-Huang Transform and Its Applications*; World Scientific Publishing: Singapore, 2005; Volume 5, pp. 167–186.
28. Tucker, C.J.; Pinzón, J.E.; Brown, M.E. Global Inventory Modeling and Mapping Studies, NA94apr15b. n11-VIg, 2.0; In *Global Land Cover Facility*; University of Maryland: College Park, MD, USA, 2004.
29. Tucker, C.J.; Pinzón, J.E.; Brown, M.E.; Slayback, D.A.; Pak, E.W.; Mahoney, R.; Vermote, E.F.; El Saleous, N. An extended AVHRR 8-km NDVI dataset compatible with MODIS and SPOT vegetation NDVI data. *Int. J. Remote Sens.* **2005**, *26*, 4485–4498.
30. Fensholt, R.; Langanke, T.; Rasmussen, K.; Reenberg, A.; Prince, S.D.; Tucker, C.; Scholes, R.J.; Le, Q.B.; Bondeau, A.; Eastman, R.; et al. Greenness in semi-arid areas across the globe 1981–2007—An Earth Observing Satellite based analysis of trends and drivers. *Remote Sens. Environ.* **2012**, *121*, 144–158.
31. Beck, H.E.; McVicar, T.R.; van Dijk, A.I.J.M.; Schellekens, J.; de Jeu, R.A.M.; Bruijnzeel, L.A. Global evaluation of four AVHRR-NDVI data sets: Intercomparison and assessment against Landsat imagery. *Remote Sens. Environ.* **2011**, *115*, 2547–2563.

32. Fensholt, R.; Proud, S.R. Evaluation of earth observation based global long term vegetation trends-comparing GIMMS and MODIS global NDVI time series. *Remote Sens. Environ.* **2012**, *119*, 131–147.
33. Bai, Z.; Dent, D. Recent land degradation and improvement in China. *Ambio* **2009**, *38*, 150–156.
34. Helldén, U.; Tottrup, C. Regional desertification: A global synthesis. *Glob. Planet. Chang.* **2008**, *64*, 169–176.
35. Zhu, Z.; Bi, J.; Pan, Y.; Ganguly, S.; Anav, A.; Xu, L.; Samanta, A.; Piao, S.; Nemani, R.R.; Myneni, R.B. Global data sets of vegetation Leaf Area Index (LAI)3g and Fraction of Photosynthetically Active Radiation (FPAR)3g derived from Global Inventory Modeling and Mapping Studies (GIMMS) Normalized Difference Vegetation Index (NDVI3g) for the period 1981 to 2011. *Remote Sens.* **2013**, *5*, 927–948.
36. Yuan, H.; Dai, Y.; Xiao, Z.; Ji, D.; Shangguan, W. Reprocessing the MODIS Leaf Area Index products for land surface and climate modelling. *Remote Sens. Environ.* **2011**, *115*, 1171–1187.
37. Baret, F.; Hagolle, O.; Geiger, B.; Bicheron, P.; Miras, B.; Huc, M.; Berthelot, B.; Niño, F.; Weiss, M.; Samain, O.; *et al.* LAI, fAPAR and fCover CYCLOPES global products derived from VEGETATION: Part 1: Principles of the algorithm. *Remote Sens. Environ.* **2007**, *110*, 275–286.
38. Liu, S.; Liu, R.; Liu, Y. Spatial and temporal variation of global LAI during 1981–2006. *J. Geogr. Sci.* **2010**, *20*, 323–332.
39. Poulter, B.; Pederson, N.; Liu, H.; Zhu, Z.; D'Arrigo, R.; Ciais, P.; Davi, N.; Frank, D.; Leland, C.; Myneni, R.; *et al.* Recent trends in Inner Asian forest dynamics to temperature and precipitation indicate high sensitivity to climate change. *Agr. For. Meteorol.* **2013**, doi: 10.1016/j.agrformet.2012.12.006.
40. Xiao, J.; Moody, A. Trends in vegetation activity and their climatic correlates: China 1982 to 1998. *Int. J. Remote Sens.* **2004**, *25*, 5669–5689.
41. Evans, J.; Geerken, R. Discrimination between climate and human-induced dryland degradation. *J. Arid Environ.* **2004**, *57*, 535–554.
42. Pettorelli, N.; Vik, J.O.; Mysterud, A.; Gaillard, J.M.; Tucker, C.J.; Stenseth, N.C. Using the satellite-derived NDVI to assess ecological responses to environmental change. *Trends Ecol. Evol.* **2005**, *20*, 503–510.
43. Scurlock, J.M.O.; Johnson, K.; Olson, R.J. Estimating net primary productivity from grassland biomass dynamics measurements. *Glob. Chang. Biol.* **2002**, *8*, 736–753.
44. Meiyappan, P.; Jain, A.K. Three distinct global estimates of historical land-cover change and land-use conversions for over 200 years. *Front. Earth Sci.* **2012**, *6*, 122–139.
45. Houghton, R.A. Carbon Flux to the Atmosphere from Land Use Changes: 1850–2005. In *A Compendium of Data on Global Change*; Carbon Dioxide Information Analysis Center, Oak Ridge National Laboratory, US Department of Energy: Oak Ridge, TN, USA, 2008.
46. Klein Goldewijk, K.; Beusen, A.; van Drecht, G.; de Vos, M. The HYDE 3.1 spatially explicit database of human-induced global land-use change over the past 12,000 years. *Glob. Ecol. Biogeogr.* **2011**, *20*, 73–86.
47. Ramankutty, N.; Foley, J.A. Estimating historical changes in global land cover: Croplands from 1700 to 1992. *Glob. Biogeochem. Cy.* **1999**, *13*, 997–1027.

48. Jain, A. Global Historical Land-Cover Change and Land-Use Conversions. Available online: <http://www.atmos.illinois.edu/meiyapp2/datasets.htm> (accessed on 15 May 2013).
49. Food and Agriculture Organization of the United Nations (FAO). *FAOSTAT Technical Report*; FAO: Rome, Italy, 2008.
50. Mitchell, T.D.; Jones, P.D. An improved method of constructing a database of monthly climate observations and associated high-resolution grids. *Int. J. Climatol.* **2005**, *25*, 693–712.
51. Berry, J.; Bjorkman, O. Photosynthetic response and adaptation to temperature in higher plants. *Ann. Rev. Plant Physiol.* **1980**, *31*, 491–543.
52. Manzano, M.G.; Návar, J. Processes of desertification by goats overgrazing in the Tamaulipan thornscrub (matorral) in north-eastern Mexico. *J. Arid Environ.* **2000**, *44*, 1–17.
53. Orlovsky, L.; Kogan, F.; Eshed, E.; Dugarjav, C. Monitoring Droughts and Pastures Productivity in Mongolia Using NOAA-AVHRR Data; In *Use of Satellite and In-Situ Data to Improve Sustainability*; Kogan, F., Powell, A., Fedorov, O., Eds.; NATO Science for Peace and Security Series C: Environmental Security; Springer: Dordrecht, The Netherlands, 2011; pp. 69–79.
54. Myneni, R.; Keeling, C.; Tucker, C.; Asrar, G.; Nemani, R. Increased plant growth in the northern high latitudes from 1981 to 1991. *Nature* **1997**, *386*, 698–702.
55. Goetz, S.J.; Bunn, A.G.; Fiske, G.J.; Houghton, R.A. Satellite-observed photosynthetic trends across boreal North America associated with climate and fire disturbance. *Proc. Natl. Acad. Sci. USA* **2005**, *102*, 13521–13525.
56. Xu, L.; Myneni, R.B.; Chapin III, F.S.; Callaghan, T.V.; Pinzon, J.E.; Tucker, C.J.; Zhu, Z.; Bi, J.; Ciais, P.; Tommervik, H.; et al. Temperature and vegetation seasonality diminishment over northern lands. *Nat. Clim. Chang.* **2013**, doi: 10.1038/nclimate1836.
57. Hickler, T.; Eklundh, L.; Seaquist, J.W.; Smith, B.; Ardö, J.; Olsson, L.; Sykes, M.; Sjöström, M. Precipitation controls Sahel greening trend. *Geophys. Res. Lett.* **2005**, *32*, L21415.
58. Olsson, L.; Eklundh, L.; Ardö, J. A recent greening of the Sahel-trends, patterns and potential causes. *J. Arid Environ.* **2005**, *63*, 556–566.
59. Wessels, K.J. Letter to the editor, comments on "Proxy gobal assessment of land degradation" by Bai *et al.* (2008). *Soil Use Manag.* **2009**, *25*, 91–92.
60. Brogaard, S.; Xueyong, Z. Rural reforms and changes in land management and attitudes: A case study from Inner Mongolia, China. *Ambio* **2002**, *31*, 219–225.
61. Thwaites, R.; de Lacy, T.; Hong, L.Y.; Hua, L.X. Property rights, social change, and grassland degradation in Xilingol Biosphere Reserve, Inner Mongolia, China. *Soc. Nat. Resour.* **1998**, *11*, 319–338.
62. Hicke, J.A.; Asner, G.P.; Randerson, J.T.; Tucker, C.; Los, S.; Birdsey, R.; Jenkins, J.C.; Field, C. Trends in North American net primary productivity derived from satellite observations, 1982–1998. *Glob. Biogeochem. Cy.* **2002**, *16*, doi: 10.1029/2001GB001550.
63. Van Dijk, A.I.J.M.; Beck, H.E.; Crosbie, R.S.; de Jeu, R.A.M.; Liu, Y.Y.; Podger, G.M.; Timbal, B.; Viney, N.R. The millennium drought in southeast Australia (2001–2009): Natural and human causes and implications for water resources, ecosystems, economy, and society. *Water Resour. Res.* **2013**, doi: 10.1002/wrcr.20123.

64. Donohue, R.J.; McVicar, T.R.; Roderick, M.L. Climate-related trends in Australian vegetation cover as inferred from satellite observations, 1981–2006. *Glob. Chang. Biol.* **2009**, *15*, 1025–1039.
65. McGrath, G.S.; Sadler, R.; Fleming, K.; Tregoning, P.; Hinz, C.; Veneklaas, E.J. Tropical cyclones and the ecohydrology of Australia’s recent continental-scale drought. *Geophys. Res. Lett.* **2012**, doi: 10.1029/2011GL050263.
66. Zhao, M.; Running, S.W. Drought-induced reduction in global terrestrial net primary production from 2000 through 2009. *Science* **2010**, *329*, 940–943.
67. Fernández, O.A.; Gil, M.E.; Distel, R.A. The challenge of rangeland degradation in a temperate semiarid region of Argentina: The Caldenal. *Land Degrad. Dev.* **2009**, *20*, 431–440.
68. Munyati, C.; Makgale, D. Multitemporal Landsat TM imagery analysis for mapping and quantifying degraded rangeland in the Bahurutshe communal grazing lands, South Africa. *Int. J. Remote Sens.* **2009**, *30*, 3649–3668.
69. Paudel, K.P.; Andersen, P. Assessing rangeland degradation using multi temporal satellite images and grazing pressure surface model in Upper Mustang, Trans Himalaya, Nepal. *Remote Sens. Environ.* **2010**, *114*, 1845–1855.
70. Le, Q.B.; Tamene, L.; Vlek, P.L. Multi-pronged assessment of land degradation in West Africa to assess the importance of atmospheric fertilization in masking the processes involved. *Glob. Planet. Chang.* **2012**, *92–93*, 71–81.
71. Ainsworth, E.A.; Long, S.P. What have we learned from 15 years of free-air CO₂ enrichment (FACE)? A meta-analytic review of the responses of photosynthesis, canopy properties and plant production to rising CO₂. *New Phytol.* **2005**, *165*, 351–372.
72. Ainsworth, E.A.; Rogers, A. The response of photosynthesis and stomatal conductance to rising CO₂: Mechanisms and environmental interactions. *Plant Cell Environ.* **2007**, *30*, 258–270.
73. Los, S.O. Analysis of trends in fused AVHRR and MODIS NDVI data for 1982–2006: Indication for a CO₂ fertilization effect in global vegetation. *Glob. Biogeochem. Cy.* **2013**, doi: 10.1002/gbc.20027.
74. Piao, S.; Friedlingstein, P.; Ciais, P.; Zhou, L.; Chen, A. Effect of climate and CO₂ changes on the greening of the Northern Hemisphere over the past two decades. *Geophys. Res. Lett.* **2006**, doi: 10.1029/2006GL028205.
75. Hickler, T.; Smith, B.; Prentice, I.C.; Mjöfors, K.; Miller, P.; Arneth, A.; Sykes, M.T. CO₂ fertilization in temperate FACE experiments not representative of boreal and tropical forests. *Glob. Chang. Biol.* **2008**, *14*, 1531–1542.
76. Oechel, W.C.; Cowles, S.; Grulke, N.; Hastings, S.J.; Lawrence, B.; Prudhomme, T.; Riechers, G.; Strain, B.; Tissue, D.; Vourlitis, G. Transient nature of CO₂ fertilization in Arctic tundra. *Nature* **1994**, *371*, 500–503.
77. Reich, P.B.; Hobbie, S.E. Decade-long soil nitrogen constraint on the CO₂ fertilization of plant biomass. *Nat. Clim. Chang.* **2013**, *3*, 278–282.
78. Archer, S.; Schimel, D.; Holland, E. Mechanisms of shrubland expansion: Land use, climate or CO₂? *Clim. Chang.* **1995**, *29*, 91–99.
79. Naito, A.T.; Cairns, D.M. Patterns and processes of global shrub expansion. *Progr. Phys. Geogr.* **2011**, *35*, 423–442.

80. Archer, S.; Boutton, T.W.; Hibbard, K. 1.9 - Trees in Grasslands: Biogeochemical Consequences of Woody Plant Expansion. In *Global Biogeochemical Cycles in the Climate System*; Schulze, E.D., Heimann, M., Harrison, S., Holland, E., Lloyd, J., Prentice, I.C., Schimel, D., Eds.; Academic Press: San Diego, CA, USA, 2001; pp. 115–137.
81. Eldridge, D.J.; Bowker, M.A.; Maestre, F.T.; Roger, E.; Reynolds, J.F.; Whitford, W.G. Impacts of shrub encroachment on ecosystem structure and functioning: Towards a global synthesis. *Ecol. Lett.* **2011**, *14*, 709–722.
82. Briggs, J.M.; Knapp, A.K.; Blair, J.M.; Heisler, J.L.; Hoch, G.A.; Lett, M.S.; McCarron, J.K. An ecosystem in transition: Causes and consequences of the conversion of mesic grassland to shrubland. *BioScience* **2005**, *55*, 243–254.
83. Lett, M.S.; Knapp, A.K.; Briggs, J.M.; Blair, J.M. Influence of shrub encroachment on aboveground net primary productivity and carbon and nitrogen pools in a mesic grassland. *Can. J. Bot.* **2004**, *82*, 1363–1370.
84. Maestre, F.T.; Bowker, M.A.; Puche, M.D.; Belén Hinojosa, M.; Martínez, I.; García-Palacios, P.; Castillo, A.P.; Soliveres, S.; Luzuriaga, A.L.; Sánchez, A.M.; *et al.* Shrub encroachment can reverse desertification in semi-arid Mediterranean grasslands. *Ecol. Lett.* **2009**, *12*, 930–941.
85. Knapp, A.K.; Briggs, J.M.; Collins, S.L.; Archer, S.R.; Bret-Harte, M.S.; Ewers, B.E.; Peters, D.P.; Young, D.R.; Shaver, G.R.; Pendall, E.; *et al.* Shrub encroachment in North American grasslands: Shifts in growth form dominance rapidly alters control of ecosystem carbon inputs. *Glob. Chang. Biol.* **2008**, *14*, 615–623.
86. Goetz, S.J.; Fiske, G.J.; Bunn, A.G. Using satellite time-series data sets to analyze fire disturbance and forest recovery across Canada. *Remote Sens. Environ.* **2006**, *101*, 352–365.
87. De Jong, R.; de Bruin, S.; Schaepman, M.; Dent, D. Quantitative mapping of global land degradation using Earth observations. *Int. J. Remote Sens.* **2011**, *32*, 6823–6853.
88. Bai, Z.; Dent, D. Recent land degradation and improvement in China. *Ambio* **2009**, *38*, 150–156.
89. Wessels, K.; Prince, S.; Malherbe, J.; Small, J.; Frost, P.; VanZyl, D. Can human-induced land degradation be distinguished from the effects of rainfall variability? A case study in South Africa. *J. Arid Environ.* **2007**, *68*, 271–297.

© 2013 by the authors; licensee MDPI, Basel, Switzerland. This article is an open access article distributed under the terms and conditions of the Creative Commons Attribution license (<http://creativecommons.org/licenses/by/3.0/>).